NTNU – Trondheim
Norwegian University of
Science and Technology

Divergence-free Isogeometric Methods for Flow in Porous Media

Jens Birkevold

Master of Science in Physics and Mathematics
Submission date: July 2012
Supervisor: Trond Kvamsdal, MATH
Co-supervisor: Knut-Andreas Lie, SINTEF

Norwegian University of Science and Technology
Department of Mathematical Sciences

Abstract

This thesis is focused on solving the Darcy flow problem using divergence-free isogeometric methods, and comparing these results to the ones obtained using traditional finite element methods with Taylor Hood elements. A short introduction to B-splines is given, and a chapter is also about using repeated knots in the knot vectors to obtain a discontinuous basis for the finite element method. This can be useful when dealing with varying permeabilities.

Sammendrag

Denne oppgaven tar for seg numerisk løsning av Darcy strømning ved bruk av divergensfrie isogeometriske metoder, og sammenligning av resultatene med de vi får fra tradisjonelle elementmetoder ved bruk av Taylor Hood elementer. En kort introduksjon til B-splines er også med, samt et kapittel om bruk av repeterte knutepunkt i knutepunktsvektorene for å oppnå ikke-kontinuerlige basiser for elementmetoden. Dette er nyttig i forbindelse med varierende permeabiliteter.

Preface

This thesis is the final work of my education to become a Master of Science in Physics and Mathematics (sivilingeniør) with specialization in Industrial Mathematics. My last two years have been focused on the field of numerics, and this thesis is about the use of the finite element method with B-splines as basis functions.

First of all I would like to thank my supervisors Trond Kvamsdal and Knut-Andreas Lie for guiding me through this thesis. Our many talks have inspired and motivated me. I am also very grateful to Kjetil André Johannessen who has helped me with the programming.

My first encounter with the use of B-splines in the finite element method was in my summer internship at SINTEF ICT in 2011. This led to my specialization project in the fall of 2011, which this master thesis is based on. The thesis is written in collaboration with SINTEF and NTNU.

Last but not least I would like to thank my fiancée Tonje for being supportive and understanding during late working ours.

Jens Birkevold
June 2012

Contents

Chapter 1

Introduction

In this thesis our main goal is to calculate flow through porous media. We will focus on the finite element method, and the use of different basis function. We will compare Taylor-Hood elements to the use of compatible B-splines, which is expected to give a divergence-free numerical solution.

The idea is that compatible B-splines in the future could be used in reservoar simulations, since they provide a divergence-free numerical solution and it is possible to alter the regularity at element boundaries. The latter property is particularly interesting when dealing with sudden changes in the permeability of the porous media. A typical geological model of a reservoar will give the permeability a constant value in each element, and the differences between neighboring elements can be quite substancial.

The theory in this thesis is based on the specialization project of Jens Birkevold, which again is inspired by the work of John A. Evans [8], [9], [10] and [7]. While the focus of the specialization project was to give an introduction to the theory of compatible B-splines, the focus of this thesis has been to make a working MATLAB implementation of this theory. Therefore there is not so much new theory in this thesis, but some of the theory from the specialization project has been included to make it complete. This has been approved of the supervisor.

Chapter 2

B-splines

2.1 B-splines

Definition of the B-splines, from Cottrell, Hughes and Bazilevs [4]:

$$N_{i,0}(\xi) = \begin{cases} 1 & \text{if } \xi_i \leq \xi < \xi_{i+1} \\ 0 & \text{otherwise} \end{cases} \tag{2.1}$$

$$N_{i,p}(\xi) = \frac{\xi - \xi_i}{\xi_{i+p} - \xi_i} N_{i,p-1}(\xi) + \frac{\xi_{i+p+1} - \xi}{\xi_{i+p+1} - \xi_{i+1}} N_{i+1,p-1}(\xi) \tag{2.2}$$

where $\Xi = [\xi_i]$, $i = 1, \ldots, n+p+1$, is the knot vector, and p is the polynomial order. If $\xi_{i+p} - \xi_i = 0$, $\frac{\xi - \xi_i}{\xi_{i+p} - \xi_i}$ is taken to be zero, and $\frac{\xi_{i+p+1} - \xi}{\xi_{i+p+1} - \xi_{i+1}}$ is taken to be zero whenever $\xi_{i+p+1} - \xi_{i+1} = 0$. Open knotvectors have the first $p+1$ entries equal and also the $p+1$ last entries equal. For all of them we require $\xi_i \leq \xi_{i+1}$.

We also define the vector $\boldsymbol{\zeta} = \{\zeta_1, \ldots, \zeta_m\}$ which contains the knots of Ξ but without repetition, and the corresponding vector $\mathbf{r} = \{r_1, \ldots, r_m\}$ where r_i is the multiplicity of ζ_i in Ξ. The regularity vector $\boldsymbol{\alpha} = \{\alpha_1, \ldots, \alpha_m\}$ is defined as; $\alpha_i = p - r_i$. We will also have use for the vector $\boldsymbol{\alpha} - 1$ which is defined to be $\boldsymbol{\alpha} - 1 = \{-1, \alpha_2 - 1, \ldots, \alpha_{m-1} - 1, -1\}$.

More information about B-splines can be found in Lyche and Mørken [14].

2.1.1 An example

Lets make the 2nd order B-splines from the knot vector

$$\Xi = \left[0 \;\; 0 \;\; 0 \;\; \frac{1}{2} \;\; 1 \;\; 1 \;\; 1\right]. \tag{2.3}$$

The 0th order B-splines, by equation (2.1) becomes:

$$N_{1,0}(\xi) = 0$$

$$N_{2,0}(\xi) = 0$$

$$N_{3,0}(\xi) = \begin{cases} 1 & 0 < \xi < 1/2 \\ 0 & \text{otherwise} \end{cases}$$

$$N_{4,0}(\xi) = \begin{cases} 1 & 1/2 < \xi < 1 \\ 0 & \text{otherwise} \end{cases}$$

$$N_{5,0}(\xi) = 0$$

$$N_{6,0}(\xi) = 0$$

The 1st order B-splines can be found by using equation (2.2);

$$N_{1,1}(\xi) = 0$$

$$N_{2,1}(\xi) = \begin{cases} 1 - 2\xi & 0 < \xi < 1/2 \\ 0 & \text{otherwise} \end{cases}$$

$$N_{3,1}(\xi) = \begin{cases} 2\xi & 0 < \xi < 1/2 \\ 2(1-\xi) & 1/2 < \xi < 1 \\ 0 & \text{otherwise} \end{cases}$$

$$N_{4,1}(\xi) = \begin{cases} 2\xi - 1 & 1/2 < \xi < 1 \\ 0 & \text{otherwise} \end{cases}$$

$$N_{5,1}(\xi) = 0$$

And finally the 2nd order B-splines, also by equation (2.2);

$$N_{1,2}(\xi) = \begin{cases} (1 - 2\xi)^2 & 0 < \xi < 1/2 \\ 0 & \text{otherwise} \end{cases}$$

$$N_{2,2}(\xi) = \begin{cases} 2\xi(2 - 3\xi) & 0 < \xi < 1/2 \\ 2(1-\xi)^2 & 1/2 < \xi < 1 \\ 0 & \text{otherwise} \end{cases}$$

$$N_{3,2}(\xi) = \begin{cases} 2\xi^2 & 0 < \xi < 1/2 \\ 8\xi - 6\xi^2 - 2 & 1/2 < \xi < 1 \\ 0 & \text{otherwise} \end{cases}$$

$$N_{4,2}(\xi) = \begin{cases} (2\xi - 1)^2 & 1/2 < \xi < 1 \\ 0 & \text{otherwise} \end{cases}$$

A plot of the 2nd order B-splines can be found in Figure 2.1.

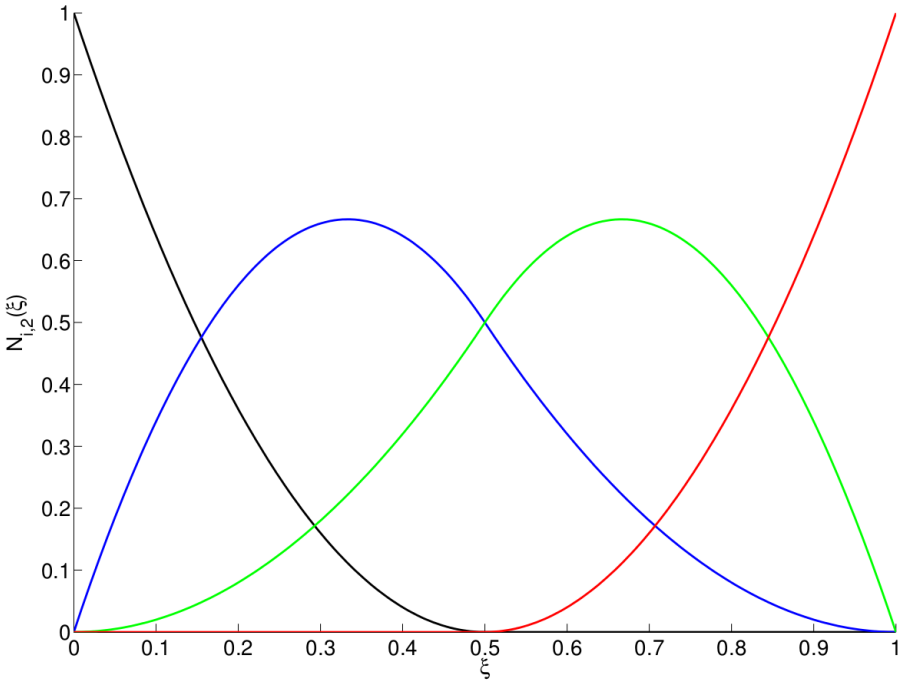

Figure 2.1: 2nd order B-splines made from knot vector given in (2.3).

2.1.2 B-spline curves

To make a B-spline curve $\mathbf{C}$ each B-spline must be mulitplied with a control point $\mathbf{P}_i$ and summarized like this:

$$\mathbf{C}(\xi) = \sum_{i=1}^{n} N_{i,p}(\xi)\mathbf{P}_i \tag{2.4}$$

An example of a B-spline curve is given in Figure 2.2.

2.1.3 B-spline surfaces

A B-spline surface is created almost the same way as a B-spline curve, but with a B-spline basis function in each direction, like this:

$$\mathbf{S}(\xi, \eta) = \sum_{i=1}^{n}\sum_{j=1}^{m} N_{i,p_1}(\xi)N_{j,p_2}(\eta)\mathbf{P}_{i,j} \tag{2.5}$$

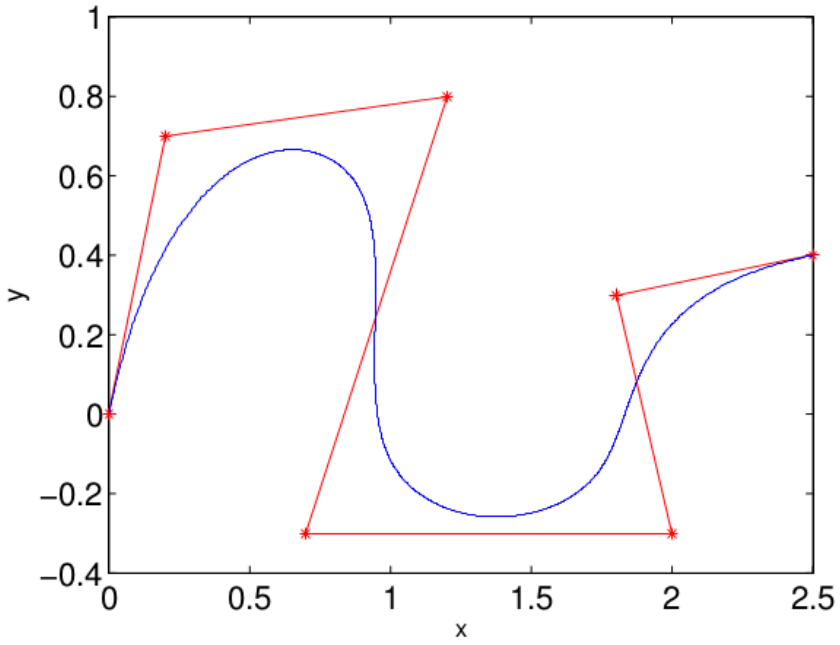

Figure 2.2: The blue line is a B-spline curve of order 2, and the red dots are the control points.

2.2 Derivatives of B-splines

The derivatives of these B-splines can be expressed as

$$N'_{i,p}(\xi) = \frac{p}{\xi_{i+p} - \xi_i} N_{i,p-1}(\xi) - \frac{p}{\xi_{i+p+1} - \xi_{i+1}} N_{i+1,p-1}(\xi), \tag{2.6}$$

as derived in Piegl and Tiller [16] and Rogers [17].

2.3 Repeated knots

In order to reduce the regularity at some knots, one may repeat this knot in the knot vector. If you repeat the knot p times, the resulting curve will be C^0 continous, and perhaps more relevant for our examples later; if the knot is repeated $p + 1$ times, the curve will be discontinuous at this knot. See Figure 2.3.

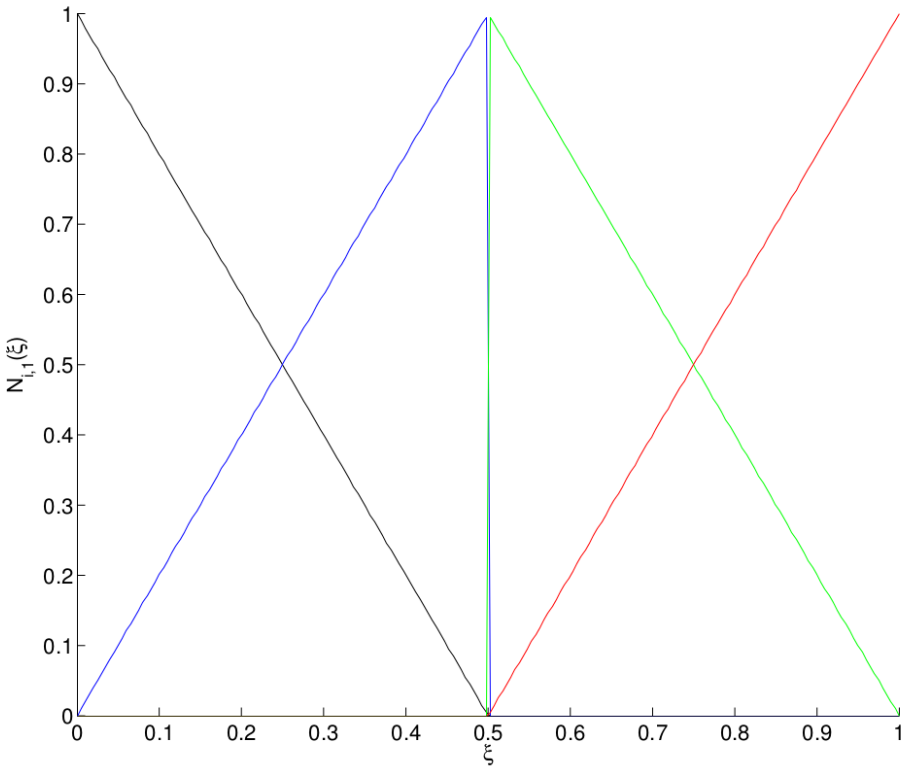

Figure 2.3: B-splines constructed of order 1 contructed from the knot vector $\left[0\ 0\ \frac{1}{2}\ \frac{1}{2}\ 1\ 1\right]$.

Chapter 3

Taylor Hood elements

In this chapter and the next we will solve the Darcy flow problem using two different methods. First we will use the finite element method with Taylor Hood elements and then in the next chapter we will use the finite element method with B-splines.

3.1 General

The Darcy flow problem, here formulated for a divergence-free (incompressible) fluid and with homogenous boundary conditions, is

$$\begin{aligned} \mathbf{u} + \nabla p &= \mathbf{f} \quad \text{in } \Omega && \text{(3.1a)} \\ \nabla \cdot \mathbf{u} &= 0 \quad \text{in } \Omega && \text{(3.1b)} \\ \mathbf{u} &= \mathbf{0} \quad \text{on } \partial\Omega && \text{(3.1c)} \end{aligned}$$

where $\mathbf{u}$ is the velocity and p is the pressure, and $\mathbf{u} : \Omega \to \mathbb{R}^2$ and $\mathbf{f} : \Omega \to \mathbb{R}^2$.

We are going to solve this using the finite element method with quadrilateral elements, and it is important that the approximation spaces for the velocity and the pressure, $\mathcal{U}_h$ and $\mathcal{L}_h$ respectively, satisfies the LBB-condition (after Ladyzenskaya, Babuska, Brezzi), or sometimes called just the Babuska-Brezzi-condition:

$$\inf_{q \in \mathcal{L}_h} \sup_{\mathbf{v} \in \mathcal{U}_h} \frac{b(q, \mathbf{v})}{||q||_{\mathcal{L}_h} ||\mathbf{v}||_{\mathcal{U}_h}} \geq \beta \tag{3.2}$$

for some $\beta > 0$.

Here we are going use Taylor-Hood elements, that is, we will use quadrilateral Lagrange elements with biquadratic shape functions for the velocity and bilinear shape functions for the pressure. The location of the nodes for both pressure and velocity is shown on Figure 3.1 below. These elements satisfies the LBB-condition (3.2), see [6] and [11]. The

problem with this choice of elements and basis functions, is that we end up with too few conditions for (3.1b) which results in a solution that does not satisfy this condition in every point, because the approximation space for the velocity is too big compared to the approximation space for the pressure. We shall later see a better choice of approximation spaces.

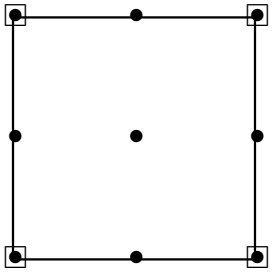

Figure 3.1: A Taylor-Hood element. A bullet indicates a node for the velocity, and a square indicates a node for the pressure.

To perform numerical integration over all elements it is necessary to create a reference

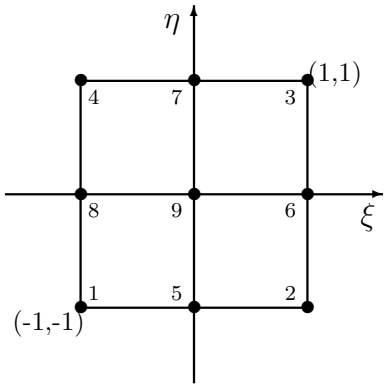

Figure 3.2: A reference element with node numbers.

element, which there exists mappings to from each of the elements. The integration can be done in this element and the result mapped back to the physical element. Figure 3.2 shows the reference element. Each of the 9 quadratic basis functions, φ_i, for this element

is given below:

$$\begin{aligned}
\varphi_1(\xi,\eta) &= \frac{1}{4}\xi(\xi-1)\eta(\eta-1)\\
\varphi_2(\xi,\eta) &= \frac{1}{4}\xi(\xi+1)\eta(\eta-1)\\
\varphi_3(\xi,\eta) &= \frac{1}{4}\xi(\xi+1)\eta(\eta+1)\\
\varphi_4(\xi,\eta) &= \frac{1}{4}\xi(\xi-1)\eta(\eta+1)\\
\varphi_5(\xi,\eta) &= -\frac{1}{2}(\xi-1)(\xi+1)\eta(\eta-1)\\
\varphi_6(\xi,\eta) &= -\frac{1}{2}\xi(\xi+1)(\eta-1)(\eta+1)\\
\varphi_7(\xi,\eta) &= -\frac{1}{2}(\xi-1)(\xi+1)\eta(\eta+1)\\
\varphi_8(\xi,\eta) &= -\frac{1}{2}\xi(\xi-1)(\eta-1)(\eta+1)\\
\varphi_9(\xi,\eta) &= (\xi-1)(\xi+1)(\eta-1)(\eta+1),
\end{aligned}$$

and the linear basis functions, ψ_i,

$$\begin{aligned}
\psi_1(\xi,\eta) &= \frac{1}{4}(\xi-1)(\eta-1)\\
\psi_2(\xi,\eta) &= -\frac{1}{4}(\xi+1)(\eta-1)\\
\psi_3(\xi,\eta) &= \frac{1}{4}(\xi+1)(\eta+1)\\
\psi_4(\xi,\eta) &= -\frac{1}{4}(\xi-1)(\eta+1).
\end{aligned}$$

First we need to transform (3.1) to weak form, which is done by multiplying (3.1a) by a test function $\mathbf{v} \in \mathbf{H}_0^1(\Omega)$ and (3.1b) by $q \in L^2(\Omega)$, and integrate over Ω. This results in:

Find $\mathbf{u} \in \mathbf{H}_0^1(\Omega)$ and $L^2(\Omega)$ such that

$$a(\mathbf{u},\mathbf{v}) - b(p,\mathbf{v}) = (\mathbf{f},\mathbf{v}) \tag{3.3}$$

$$b(q,\mathbf{u}) = 0 \tag{3.4}$$

for all $\mathbf{v} \in \mathbf{H}_0^1(\Omega)$ and $q \in L_0^2(\Omega)$, where

$$a(\mathbf{u},\mathbf{v}) = \int_\Omega \mathbf{u}\cdot\mathbf{v}\,\mathrm{d}\Omega \tag{3.5}$$

$$b(p,\mathbf{v}) = \int_\Omega p\nabla\cdot\mathbf{v}\,\mathrm{d}\Omega. \tag{3.6}$$

To explain the minus sign in equation (3.5) and why the same b function appears in both (3.5) and (3.6) we need to look at the integral

$$\begin{aligned}\int_\Omega \nabla p \cdot \mathbf{v}\,\mathrm{d}\Omega &= \underbrace{\int_{\partial\Omega} p\mathbf{v}\cdot\mathrm{d}\mathbf{n}}_{=0} - \int_\Omega p\nabla\cdot\mathbf{v}\mathrm{d}\Omega \\ &= -\int_\Omega p\nabla\cdot\mathbf{v}\mathrm{d}\Omega.\end{aligned}$$

The second integral above is zero because $\mathbf{v}$ is assumed to be zero on the boundary $\partial\Omega$.

To discretize this we begin by introducing the function space

$$\mathcal{Q}_k = \left\{ \sum_j c_j p_j(x) q_j(y) \ : \ p_j, q_j \text{ polynomials of degree} \leq k \right\},$$

and a set of elements $\mathcal{K} = \{K_i \ : \ K_i \text{ a rectangel in } \Omega\}$. We require $\cup_i K_i = \Omega$ and $K_i \cap K_j = \emptyset$ (or the boundary between them) when $i \neq j$. Then we will restrict $\mathbf{u}$ to the space $\mathcal{U}_h = \{\mathbf{v} \in \mathbf{H}_0^1(\Omega) \ : \ v_1|_{K_i}, v_2|_{K_i} \in \mathcal{Q}_2\}$, and p to $\mathcal{L}_h = \{q \in L^2(\Omega) \ : \ q|_{K_i} \in \mathcal{Q}_1\}$.

The finite element method then becomes:

Find $\mathbf{u_h} \in \mathcal{U}_h$ and $p_h \in \mathcal{L}_h$ such that

$$a(\mathbf{u_h}, \mathbf{v_h}) - b(p_h, \mathbf{v_h}) = (\mathbf{f}, \mathbf{v_h}) \tag{3.7}$$

$$b(q_h, \mathbf{u_h}) = 0 \tag{3.8}$$

for all $\mathbf{v_h} \in \mathcal{U}_h$ and $q_h \in \mathcal{L}_h$.

Letting $u_{h1} = \sum_i U_{1i}\varphi_i$, $u_{h2} = \sum_i U_{2i}\varphi_i$ and $p_h = \sum_i P_i\psi_i$, we obtain the following linear system by using φ_i as $\mathbf{v_h}$ and ψ_i as q_h for all i in the two equations above:

$$\mathbf{AU} = \mathbf{L} \tag{3.9}$$

where

$$\mathbf{A} = \begin{bmatrix} \mathbf{K} & \mathbf{B}^T \\ \mathbf{B} & \mathbf{0} \end{bmatrix}$$

$$K_{ij} = a(\varphi_i, \varphi_j) \tag{3.10}$$

$$B_{ij} = -b(\psi_i, \varphi_j). \tag{3.11}$$

This will determine the velocity and the pressure up to a constant. Therefore we need to specify the pressure in one point in order to have a fully determined system. Rows and columns need to be removed according to the boundary conditions as well.

3.2 Implementation

The numerical solver is implemented in MATLAB. The program starts with defining all the nodes and elements, and create a mapping from local nodenumbers on the reference element (see Fig. 3.2) to the global nodenumbers, before continuing with the construction of the matrices $\mathbf{K}$ and $\mathbf{B}$. The pseudocode for this can be found in Algorithm 1.

Algorithm 1 Assembly of the matrix $\mathbf{A}$

```
zero-initialize K and B
for all elements e do
  for all non-zero functions φ_i do
    for all non-zero functions φ_j do
      K_ij = K_ij + ∫_e φ_i · φ_j
    end for
    for all non-zero functions ψ_k do
      B_ik = B_ik − ∫_e ψ_k ∇ · φ_i
    end for
  end for
end for
A = [ K   B^T ]
    [ B   0   ]
```

The unknowns U_i are organized such that all the first $(2n+1)^2$ entries in $\mathbf{U}$ corresponds to basis functions $[\varphi_i \ 0]^T$, and the next $(2n+1)^2$ corresponds to basis functions $[0 \ \varphi_i]$. The last entries corresponds to basis functions ψ_k.

After doing this we create the right hand side vector, $\mathbf{L}$, which is done in a similar way as K; just replace φ_j with $\mathbf{f}$ in the integral. The last part in $\mathbf{L}$ should be zero according to (3.1b).

The matrices should be saved as *sparse* matrices in MATLAB for bigger problems, because of the huge amount of zeros in the matrices. This will ensure shorter running time, and significant reduction in memory usage.

The integrals in Algorithm 1 is calculated by using the numerical quadrature described below.

3.2.1 Numerical integration

For the integration needed in this project Gaussian-Legendre quadrature will be used as method of numerical integration, see Kincaid [13] and Buchanan [1]. The integrals we are going to solve is products of biquadratic basis functions, so they are of order 4 (or less for the other integral of the product of a bilinear function and the dervivative of a biquadratic). An n-point Gaussian quadrature is exact for every polynomial of degree $2n-1$ or less, see [20], so it is sufficient to choose a 3-point quadrature.

The 3-point Gaussian-Legendre quadrature in one dimension is

$$\int_a^b f(x)\mathrm{d}x \approx \frac{b-a}{2}\sum_{i=1}^{3} w_i f\left(\frac{b-a}{2}x_i + \frac{a+b}{2}\right) \tag{3.12}$$

where the weights, w_i, and the points, x_i, are as given in Table 3.1.

Table 3.1: Points and weights for the one dimensional Gauss-Legendre quadrature.

Points, x_i	Weights, w_i
$-\sqrt{(3/5)}$	5/9
0	8/9
$\sqrt{(3/5)}$	5/9

The two dimensional extension of this is simply as given in Table 3.2. The formula for the two dimensional integral then becomes

$$\int_\Omega f(\mathbf{x})d\Omega \approx \sum_{i=1}^{9} w_i f(\mathbf{P}_i), \tag{3.13}$$

where Ω is the unit square, and $\mathbf{P}_i$ and w_i are the points and weigths given in Table 3.2. The same translation of the points can be done here as in the one dimensional case.

3.3 A test problem

As a test problem for (3.1), we will use $\Omega = [0,1]\times[0,1]$, and as the right hand side of equation (3.1a) we will use

$$\mathbf{f} = \begin{bmatrix} 2x^2(x-1)^2y(y-1)(2y-1) + \frac{1}{100}ye^{xy} \\ -2x(x-1)(2x-1)y^2(y-1)^2 + \frac{1}{100}xe^{xy} \end{bmatrix}. \tag{3.14}$$

Table 3.2: Points and weigths for the two dimensional Gaussian-Legendre quadrature.

Points, $\mathbf{P}_i$	Weigths, w_i
$(-\sqrt{3/5}, -\sqrt{3/5})$	25/81
$(-\sqrt{3/5}, 0)$	40/81
$(-\sqrt{3/5}, \sqrt{3/5})$	25/81
$(0, -\sqrt{3/5})$	40/81
$(0, 0)$	64/81
$(0, \sqrt{3/5})$	40/81
$(\sqrt{3/5}, -\sqrt{3/5})$	25/81
$(\sqrt{3/5}, 0)$	40/81
$(\sqrt{3/5}, \sqrt{3/5})$	25/81

This problem has the exact solution

$$\mathbf{u} = \begin{bmatrix} 2x^2(x-1)^2y(y-1)(2y-1) \\ -2x(x-1)(2x-1)y^2(y-1)^2 \end{bmatrix} \tag{3.15}$$

$$p = \frac{1}{100}e^{xy}. \tag{3.16}$$

A plot of the numerical solutions can be found in Figure 3.3. Table 3.3 shows how the L^2-norm of the divergence of $\mathbf{u}$ decreases for increasing degrees of freedom. These data is also visualised in a plot in Figure 3.4. In chapter 4 we introduce some theory that will leed up to a discretization satisfying $|\nabla \cdot \mathbf{u}| = 0$ in every point for every n.

Table 3.3: A table showing the L^2-norm of the divergence of $\mathbf{u}$ for the numerical solution with $2(2n+1)^2$ degrees of freedom.

n	$\left(\int_\Omega \lvert\nabla \cdot \mathbf{u}\rvert^2 \, \mathrm{d}\Omega\right)^{1/2}$
2	$1.12 \cdot 10^{-2}$
3	$5.78 \cdot 10^{-3}$
4	$3.56 \cdot 10^{-3}$
5	$2.50 \cdot 10^{-3}$
10	$1.09 \cdot 10^{-3}$
15	$6.55 \cdot 10^{-4}$
20	$4.91 \cdot 10^{-4}$
25	$3.93 \cdot 10^{-4}$
30	$3.29 \cdot 10^{-4}$

In Figure 3.5 there is a logarithmic plot showing the relative error, $\frac{||\mathbf{u}-\mathbf{u_h}||_2}{||\mathbf{u}||_2}$ as a function of the number of degrees of freedom together with a reference line showing quadratic

convergence. This suggests $\frac{||\mathbf{u}-\mathbf{u_h}||_2}{||\mathbf{u}||_2} = \mathcal{O}\left(\left(\frac{1}{ndof}\right)\right)$, which is supported by [5].

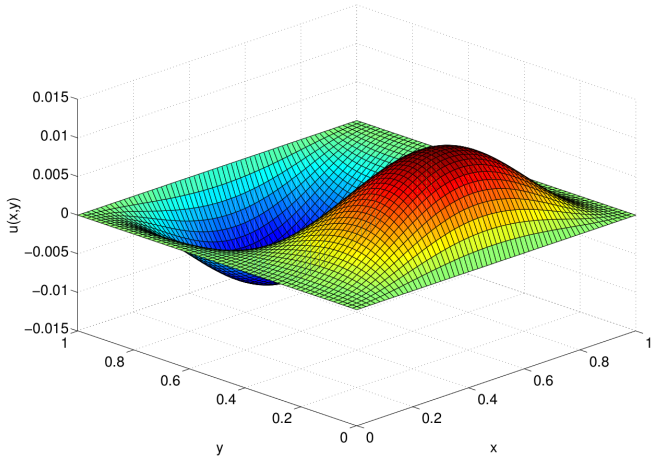

(a) u_1

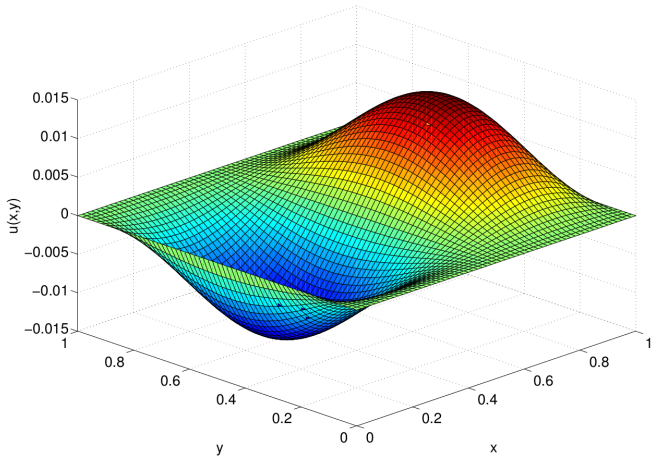

(b) u_2

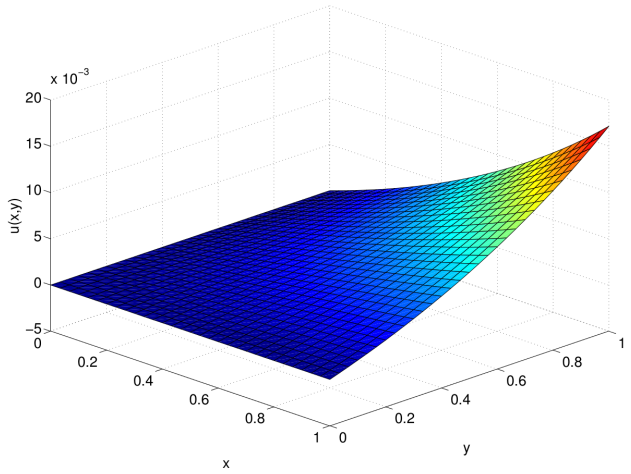

(c) p

Figure 3.3: Plots of the numerical solutions $\mathbf{u} = [u_1\ u_2]$ and p of equation (3.1) on $\Omega = [0,1] \times [0,1]$ using (3.14) as the right hand side of equation (3.1a). This solution was obtained using 900 Taylor-Hood elements.

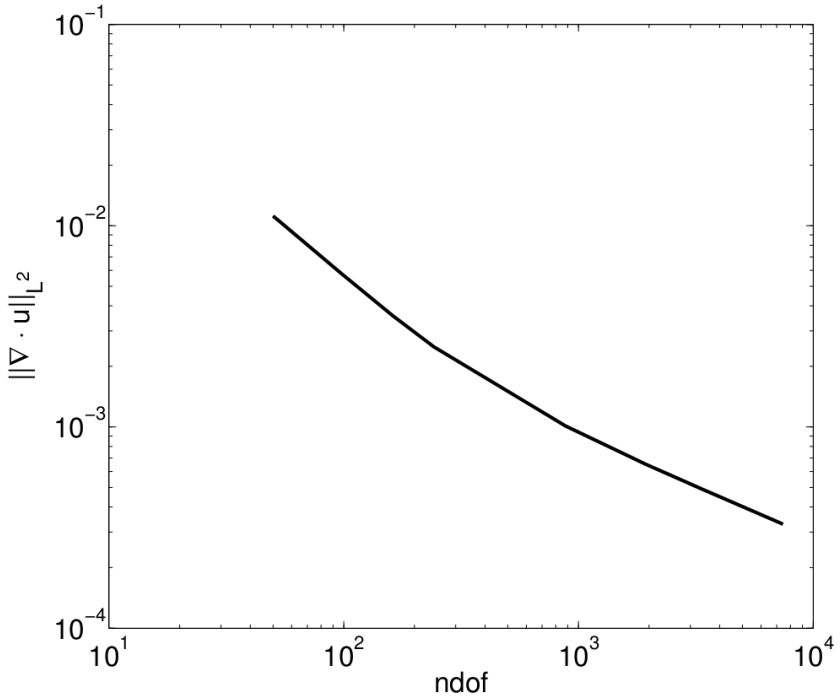

Figure 3.4: A logarithmic plot of the L^2-norm of $\nabla \cdot \mathbf{u}$ versus the number of degrees of freedom.

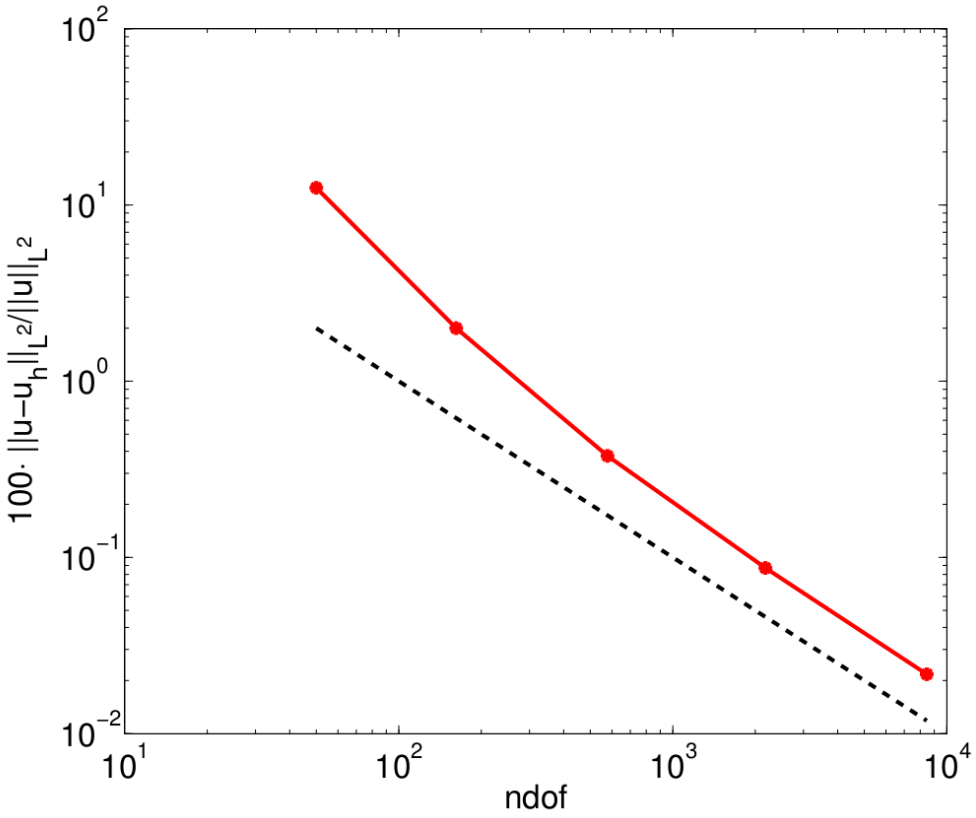

Figure 3.5: A logarithmic plot of the relative error, $\frac{||\mathbf{u}-\mathbf{u_h}||_2}{||\mathbf{u}||_2}$, in percent versus the number of degrees of freedom, $ndof$. The red line shows the datapoints, while the dotted line is a reference line showing $ndof^{-1}$.

Chapter 4

Divergence-free generalized Stokes flow

In order to improve on the finite element method in chapter 3 we will try an approach similar to the one given in Evans [8] and originally in Buffa et al. [2]. Other sources for information about this can be found in Buffa [3] and Schräder and Wendland [18], [19]. This leads to a discretization that will give a solution which will be divergence free in every point. This is because the approximation spaces has been chosen so that $\mathrm{div}\mathcal{U}_h = \mathcal{L}_h$. In [8] this is given for the generalized Stokes equation, but can be simplified to apply to the Darcy flow problem. We start here by introducing som function spaces that can become handy, before we introduce the equation and domain.

4.1 Definitions of function spaces

Here is a list of different function spaces that will come useful when we come to the Darcy flow problem. Pay especially attention to the different spline spaces which will become important.

$$
\begin{aligned}
L_0^2(\Omega) &= \left\{ q \in L^2(\Omega) : \int_\Omega q dx = 0 \right\} \\
\mathbf{L}^2(\Omega) &= \left(L^2(\Omega)\right)^3 \\
H^1(\Omega) &= \left\{ v \in L^2(\Omega) : \nabla v \in \left(L^2(\Omega)\right)^3 \right\} \\
H_0^1(\Omega) &= \{ v \in H^1(\Omega) : v = 0 \text{ on } \partial\Omega \} \\
\mathbf{H}_{\mathbf{n}}^1(\Omega) &= \{ \mathbf{v} \in \mathbf{H}^1(\Omega) : \mathbf{v} \cdot \mathbf{n} = 0 \text{ on } \partial\Omega \} \\
\mathbf{H}(\mathbf{curl}; \Omega) &= \{ \mathbf{v} \in \mathbf{L}^2(\Omega) : \nabla \times \mathbf{v} \in \mathbf{L}^2(\Omega) \} \\
\mathbf{H}_0(\mathbf{curl}; \Omega) &= \{ \mathbf{v} \in \mathbf{H}(\mathbf{curl}; \Omega) : \mathbf{v} \times \mathbf{n} = \mathbf{0} \text{ on } \partial\Omega \} \\
\mathbf{H}(\mathrm{div}; \Omega) &= \{ \mathbf{v} \in \mathbf{L}^2(\Omega) : \mathrm{div}\mathbf{v} \in L^2(\Omega) \}
\end{aligned}
$$

$$
\begin{aligned}
\mathbf{H}_0(\mathrm{div};\Omega) &= \{\mathbf{v} \in \mathbf{H}(\mathrm{div};\Omega) :\ \mathbf{v}\cdot\mathbf{n} = 0 \text{ on } \partial\Omega\} \\
\mathbf{H}^1_{\mathbf{n}}(\Omega) &= \{\mathbf{v} \in \mathbf{H}^1(\Omega) :\ \mathbf{v}\cdot\mathbf{n} = 0 \text{ on } \partial\Omega\} \\
\boldsymbol{\Phi}(\Omega) &= \{\boldsymbol{\phi} \in \mathbf{L}^2(\Omega) :\ \mathbf{curl}\boldsymbol{\phi} \in \mathbf{H}^1(\Omega)\} \\
\boldsymbol{\Phi}_{\mathbf{n}}(\Omega) &= \boldsymbol{\Phi}(\Omega) \cap \mathbf{H}_0(\mathbf{curl};\Omega) \\
\widehat{\mathcal{S}}_h &= S^{p_1,p_2,p_3}_{\boldsymbol{\alpha}_1,\boldsymbol{\alpha}_2,\boldsymbol{\alpha}_3}(\mathcal{Q}_h) \\
\widehat{\mathcal{N}}_h &= S^{p_1-1,p_2,p_3}_{\boldsymbol{\alpha}_1-1,\boldsymbol{\alpha}_2,\boldsymbol{\alpha}_3}(\mathcal{Q}_h) \times S^{p_1,p_2-1,p_3}_{\boldsymbol{\alpha}_1,\boldsymbol{\alpha}_2-1,\boldsymbol{\alpha}_3}(\mathcal{Q}_h) \times S^{p_1,p_2,p_3-1}_{\boldsymbol{\alpha}_1,\boldsymbol{\alpha}_2,\boldsymbol{\alpha}_3-1}(\mathcal{Q}_h) \\
\widehat{\mathcal{RT}}_h &= S^{p_1,p_2-1,p_3-1}_{\boldsymbol{\alpha}_1,\boldsymbol{\alpha}_2-1,\boldsymbol{\alpha}_3-1}(\mathcal{Q}_h) \times S^{p_1-1,p_2,p_3-1}_{\boldsymbol{\alpha}_1-1,\boldsymbol{\alpha}_2,\boldsymbol{\alpha}_3-1}(\mathcal{Q}_h) \times S^{p_1-1,p_2-1,p_3}_{\boldsymbol{\alpha}_1-1,\boldsymbol{\alpha}_2-1,\boldsymbol{\alpha}_3}(\mathcal{Q}_h) \\
\widehat{\mathcal{W}}_h &= S^{p_1-1,p_2-1,p_3-1}_{\boldsymbol{\alpha}_1-1,\boldsymbol{\alpha}_2-1,\boldsymbol{\alpha}_3-1}(\mathcal{Q}_h) \\
\widehat{\mathcal{S}}_{0,h} &= \widehat{\mathcal{S}}_h \cap H^1_0(\widehat{\Omega}) \\
\widehat{\mathcal{N}}_{0,h} &= \widehat{\mathcal{N}}_h \cap \mathbf{H}_0(\mathbf{curl};\widehat{\Omega}) \\
\widehat{\mathcal{RT}}_{0,h} &= \widehat{\mathcal{RT}}_h \cap \mathbf{H}_0(\mathrm{div};\widehat{\Omega})
\end{aligned}
$$

$S^{p_1,p_2,p_3}_{\boldsymbol{\alpha}_1,\boldsymbol{\alpha}_2,\boldsymbol{\alpha}_3}(\mathcal{Q}_h)$ is the tensor product B-spline space where p_d $(d = 1, 2, 3)$ is the polynomial order for the splines in each dimension, and $\boldsymbol{\alpha}_d$ is the corresponding regularity vector.

4.2 Domain

Let us denote the parametric domain as $\widehat{\Omega}$, and the physical domain as Ω. We have a piecewise smooth mapping $\mathbf{F} : \widehat{\Omega} \to \Omega$, which has a piecewise smooth inverse.

$\mathcal{Q}_h$ is a parametric Cartesian domain associated with the knot vectors.

4.3 The continuous problem

Strong form

Given $\frac{1}{\kappa} : \Omega \to \mathbb{R}$, $\nu : \Omega \to \mathbb{R}$, and $\mathbf{f} : \Omega \to \mathbb{R}^3$, find $\mathbf{u} : \bar{\Omega} \to \mathbb{R}^3$ and $p : \Omega \to \mathbb{R}$ such that

$$
\begin{aligned}
\frac{1}{\kappa}\mathbf{u} - \nabla\cdot(2\nu\nabla^s\mathbf{u}) + \nabla p &= \mathbf{f} \quad \text{in } \Omega && \text{(4.1a)} \\
\nabla\cdot\mathbf{u} &= 0 \quad \text{in } \Omega && \text{(4.1b)} \\
\mathbf{u} &= \mathbf{0} \quad \text{on } \partial\Omega && \text{(4.1c)}
\end{aligned}
$$

where

$$
\nabla^s\mathbf{u} = \frac{1}{2}\left(\nabla\mathbf{u} + (\nabla\mathbf{u})^T\right).
$$

Weak form

Find $\mathbf{u} \in \mathbf{H}_0^1(\Omega)$ and $p \in L_0^2(\Omega)$ such that

$$a(\mathbf{u}, \mathbf{v}) - b(p, \mathbf{v}) + b(q, \mathbf{u}) = (\mathbf{f}, \mathbf{v})_{\mathbf{L}^2(\Omega)} \tag{4.2}$$

for all $\mathbf{v} \in \mathbf{H}_0^1(\Omega)$ and $q \in L_0^2(\Omega)$ where

$$\begin{aligned} a(\mathbf{w}, \mathbf{v}) &= (2\nu\nabla^s\mathbf{w}, \nabla^s\mathbf{v})_{L^2(\Omega)^{3\times 3}} + (\frac{1}{\kappa}\mathbf{w}, \mathbf{v})_{\mathbf{L}^2(\Omega)}, \quad \forall \mathbf{w}, \mathbf{v} \in \mathbf{H}_0^1(\Omega) && (4.3)\\ b(q, \mathbf{v}) &= (q, \nabla \cdot \mathbf{v})_{L^2(\Omega)}, \quad \forall q \in L_0^2(\Omega),\ \mathbf{v} \in \mathbf{H}_0^1(\Omega) && (4.4) \end{aligned}$$

4.4 The discrete problem

We use

$$\mathcal{V}_{0,h} = \mathcal{RT}_{0,h} \tag{4.5}$$

as our discrete velocity space, and

$$\mathcal{Q}_{0,h} = \mathcal{W}_h \cap L_0^2(\Omega) \tag{4.6}$$

as our discrete pressure space. Since members of $\mathcal{V}_{0,h}$ only satisfy homogeneous normal Dirichlet boundary conditions and not tangential, we need to weakly enforce no-slip boundary conditions via Nietsche's method. This requires that we assume

$$\nu \in W^{1,\infty}(\Omega). \tag{4.7}$$

This leads to the following bilinear form

$$a_h(\mathbf{w}, \mathbf{v}) = a(\mathbf{w}, \mathbf{v}) - \sum_{F \in \Gamma_h} \int_F 2\nu \left(((\nabla^s\mathbf{v})\mathbf{n}) \cdot \mathbf{w} + ((\nabla^s\mathbf{w})\mathbf{n}) \cdot \mathbf{v} - \frac{C_{pen}}{h_F}\mathbf{w} \cdot \mathbf{v} \right) ds \tag{4.8}$$

where $C_{pen} > 0$ is a penalty constant, h_F is a measure of the mesh size and Γ_h is is the set of mesh faces on the boundary. All this is taken from [8]. The discrete formulation then becomes:

Find $\mathbf{u}_h \in \mathcal{V}_{0,h}$ and $p_h \in \mathcal{Q}_{0,h}$ such that

$$a_h(\mathbf{u}_h, \mathbf{v}_h) - b(p_h, \mathbf{v}_h) + b(q_h, \mathbf{u}_h) = (\mathbf{f}, \mathbf{v}_h)_{\mathbf{L}^2(\Omega)}, \quad \forall \mathbf{v}_h \in \mathcal{V}_{0,h},\ q_h \in \mathcal{Q}_{0,h} \tag{4.9}$$

4.5 De Rahm complex

Let us make some definitions:

$$p^* = \min\{p_1, p_2, p_3\}, \qquad \alpha = \min_{d=1,2,3} \min_{2 \le i \le m_d - 1} \{\alpha_{i,d}\}.$$

And let the space of piecewise smooth functions on the mesh $\mathcal{Q}_h$ with interelement regularity assigned by the vectors $\boldsymbol{\alpha}_d$ be $C^{\infty}_{\boldsymbol{\alpha}_1,\boldsymbol{\alpha}_2,\boldsymbol{\alpha}_3}(\mathcal{Q}_h)$.

The following de Rahm complex is commuting if $\alpha \ge 1$ and $\mathbf{F} \in \left(C^{\infty}_{\boldsymbol{\alpha}_1,\boldsymbol{\alpha}_2,\boldsymbol{\alpha}_3}(\mathcal{Q}_h)\right)^3$ ($\mathbf{F}$ is the mapping between the physical and the parametric domain);

$$\begin{array}{ccccccccc}
0 & \longrightarrow & H^1_0(\Omega) & \xrightarrow{\mathbf{grad}} & \boldsymbol{\Phi}_{\mathbf{n}}(\Omega) & \xrightarrow{\mathbf{curl}} & \mathbf{H}^1_{\mathbf{n}}(\Omega) & \xrightarrow{\mathrm{div}} & L^2(\Omega) & \xrightarrow{\int} & \mathbb{R} \\
 & & \Big\downarrow \Pi^0_{\mathcal{S}_h} & & \Big\downarrow \Pi^0_{\mathcal{N}_h} & & \Big\downarrow \Pi^0_{\mathcal{RT}_h} & & \Big\downarrow \Pi^0_{\mathcal{W}_h} & & \\
0 & \longrightarrow & \mathcal{S}_{0,h} & \xrightarrow{\mathbf{grad}} & \mathcal{N}_{0,h} & \xrightarrow{\mathbf{curl}} & \mathcal{RT}_{0,h} & \xrightarrow{\mathrm{div}} & \mathcal{W}_h & \xrightarrow{\int} & \mathbb{R}
\end{array}$$

where $\Pi^0_{\mathcal{S}_h}$, $\Pi^0_{\mathcal{N}_h}$, $\Pi^0_{\mathcal{RT}_h}$ and $\Pi^0_{\mathcal{W}_h}$ are quasi-interpolants given in [8].

The spline spaces in the lower line in the De Rahm complex, are called compatible B-splines. That is because the spaces are connected in the same way as the spaces for the continuous case. Using these spaces in the finite element method will ensure a divergence-free solution.

4.6 Darcy flow

If we let $\nu = 0$ the problem (4.1a) reduces to

$$\frac{1}{\kappa}\mathbf{u} + \nabla p = \mathbf{f}, \tag{4.10}$$

which is the Darcy flow problem.

The discretization described above also reduces to a discretization of incompressible Darcy flow with no-penetration boundary condition. Because $\nu = 0$, the bilinear form becomes quite simple

$$a_h(\mathbf{w}, \mathbf{v}) = (\frac{1}{\kappa}\mathbf{w}, \mathbf{v})_{\mathbf{L}^2(\Omega)}. \tag{4.11}$$

4.6.1 Formulation of the method

We need to solve

$$\begin{aligned} \frac{1}{\kappa}\mathbf{u} + \nabla p &= \mathbf{f} \quad \text{in } \Omega && (4.12a)\\ \nabla \cdot \mathbf{u} &= 0 \quad \text{in } \Omega && (4.12b)\\ \mathbf{u} &= \mathbf{0} \quad \text{on } \partial\Omega, && (4.12c) \end{aligned}$$

which is equivalent to the following weak formulation:

Find $\mathbf{u}_h \in \mathcal{V}_{0,h}$ and $p_h \in \mathcal{Q}_h$ such that

$$\begin{aligned} a(\mathbf{u}_h, \mathbf{v}_h) + b(p_h, \mathbf{v}_h) &= l(\mathbf{v}_h) && (4.13)\\ b(q_h, \mathbf{u}_h) &= 0 && (4.14) \end{aligned}$$

for all $\mathbf{v}_h \in \mathcal{V}_{0,h}$ and all $q_h \in \mathcal{Q}_{0,h}$, where

$$\begin{aligned} a(\mathbf{u}, \mathbf{v}) &= \left(\frac{1}{\kappa}\mathbf{u}, \mathbf{v}\right)_{\mathbf{L}_2(\Omega)} && (4.15)\\ b(q, \mathbf{u}) &= (q, \nabla \cdot \mathbf{u})_{L_2(\Omega)} && (4.16)\\ l(\mathbf{v}) &= (\mathbf{f}, \mathbf{v})_{\mathbf{L}_2(\Omega)} && (4.17) \end{aligned}$$

We are going to solve this in two dimensions, so we will need:

$$\begin{aligned} \mathbf{u}_x,\, \mathbf{v}_x &\in S^{p_1,p_2-1}_{\boldsymbol{\alpha}_1,\boldsymbol{\alpha}_2-1} && (4.18)\\ \mathbf{u}_y,\, \mathbf{v}_y &\in S^{p_1-1,p_2}_{\boldsymbol{\alpha}_1-1,\boldsymbol{\alpha}_2} && (4.19)\\ p, q &\in S^{p_1-1,p_2-1}_{\boldsymbol{\alpha}_1-1,\boldsymbol{\alpha}_2-1} \cap L^2_0(\Omega) && (4.20) \end{aligned}$$

We also must require that $\mathbf{u},\, \mathbf{v} \in \mathbf{L}^2(\Omega)$ and $\nabla \cdot \mathbf{u},\, \nabla \cdot \mathbf{v} \in L^2(\Omega)$, and that $\mathbf{u} \cdot \mathbf{n} = 0$ and $\mathbf{v} \cdot \mathbf{n} = 0$ on $\partial\Omega$.

In order to create a discrete equation, these functions must be expressed as a sum of B-spline basis functions;

$$\mathbf{u}_x = \sum_{i=0}^{n}\sum_{j=0}^{m} P_{i,j} N_{i,p_1}(\xi) N_{j,p_2-1}(\eta), \tag{4.21}$$

where $P_{i,j}$ is the control point corresponding to the i'th and j'th basis function in two directions respectively. Similar for the other functions mentioned above.

These basis functions only have support on a small subdomain of Ω, (more specifically

each basis function will at most have support on $p+1$ knotspans), and this will make the calculations easier.

4.7 Numerical example

The theory described earlier in this chapter has been tested on the same problem as in chapter 3.3 with great success. As described in Evans [8], we only need to consider the normal boundary conditions, since the tangential boundary conditions are automatically taken care of. We have used regular open knot vectors and no repeated knots and $p = 2$. The plot of the solution can be found in Figure 4.1.

What is interesting to observe is that opposed to the results shown in Table 3.3 for Taylor Hood elements, the solution obtained using B-splines is divergence free in every point no mather have many degrees of freedom we have. The results are not presented in a table because the L_2-norm of $\nabla \cdot \mathbf{u}$ is of order 10^{-16} (which equals zero due to machine precision) for every number of degrees of freedom.

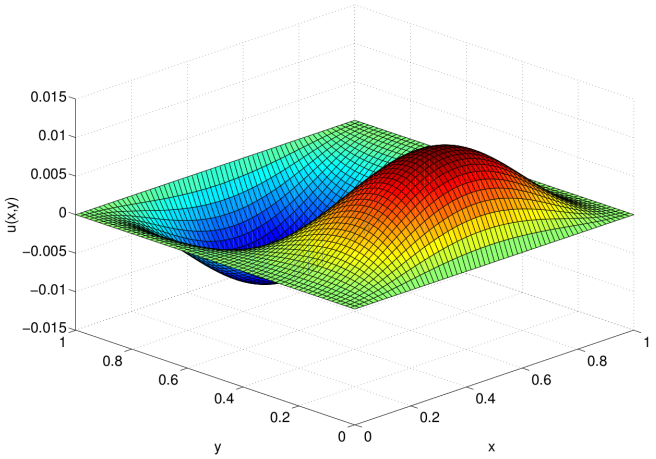

(a) u_1

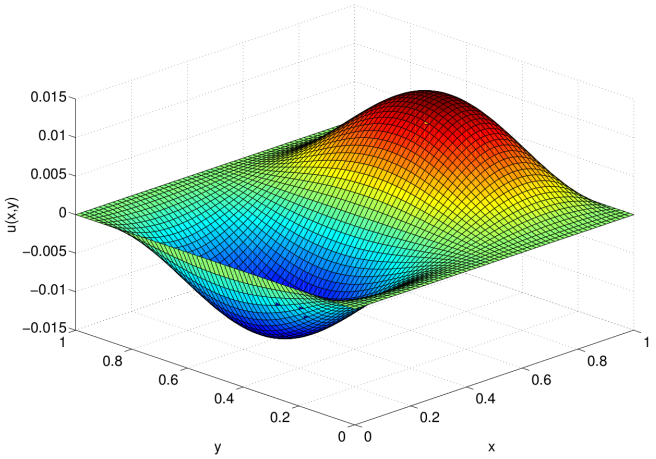

(b) u_2

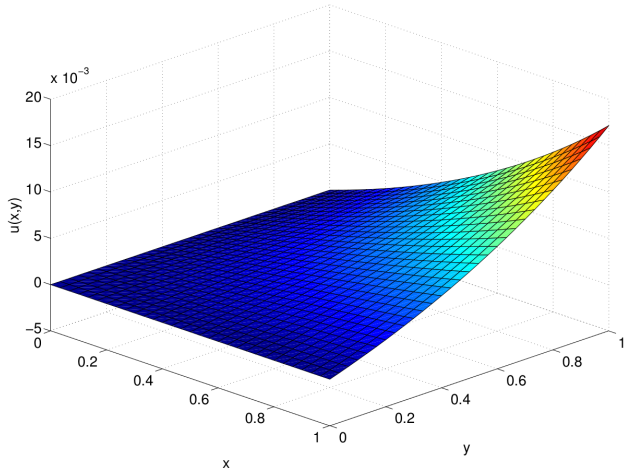

(c) p

Figure 4.1: Plots of the solution of the problem described in chapter 3.3 using B-splines in the finite element method. Calculated with 1081 degrees of freedom and $p = 2$.

Chapter 5

Numerical experiments

Another very important property of using B-splines as basis functions in the finite element method is that it is possible to control the regularity of the solution along the element boundaries. This can be useful in the case of varying permeability, κ, in the Darcy flow problem. If we have a sharp boundary between to materials with different permeability and we have a flow parallell to this boundary the velocity will be different in these materials, and we would like our numerical solution to be as correct as possible with as few elements as possible. By using just a few element we can obtain the exact solution for such a problem if we use repeated knots in the knot vector to create a basis that is discontinuous.

In these examples the boundary conditions have been imposed weakly, see Juntunen [12] and Nitsche [15].

5.1 Different permeability

We have the equation

$$\frac{1}{\kappa}\mathbf{u} + \nabla p = \mathbf{0} \tag{5.1a}$$

$$\nabla \cdot \mathbf{u} = 0 \tag{5.1b}$$

and the boundary conditions and the permeability is given in Figure 5.1. A plot of the solution can be found in Figure 5.2. As one can see the solution is exact when only a few number of elements is used. Here we have used repeated knots along the boundary between the materials in order to obtain a discontinuous solution. The sudden change in u_1 along the boundary between the two materials is so sharp because of the repeated knots. If we had used regular knot vectors without repeated knots, we would have had a more smooth transition. The same would have happened if we had used Taylor Hood

elements. Even with many degrees of freedom we would have observed some oscillations around the boundary between the materials, see Figure 5.3. u_2 is zero as expected (be aware of different scaling on the axis), and p is linear in the x-direction and constant in the y-direction.

In this example we have only used permeabilities which differ by a factor of 2, but the result is just as good for larger differences.

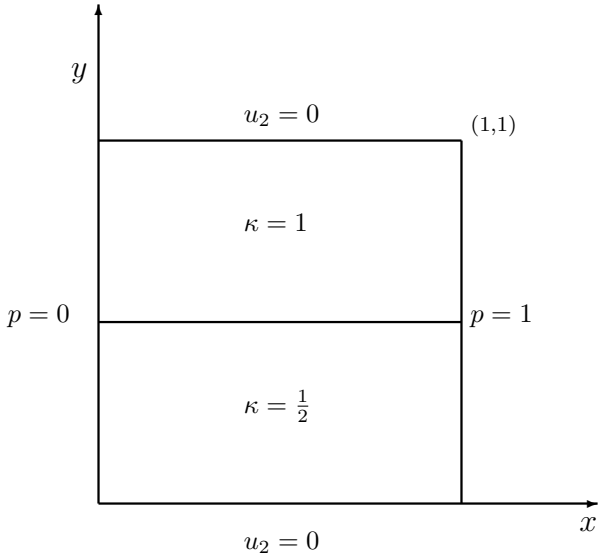

Figure 5.1: Test problem in section 5.1.

5.2 "Chess board"

A little more complicatd problem is described in Figure 5.4 and the equation is the same, see 5.1. Here we seek a solution that is discontinuous along both boundaries between the materials. This means that we use repeated knots in both x- and y-direction, and we seek a solution

$$\begin{aligned} u_1 &\in S_p^1 \times S_{p-1}^{-1} \\ u_2 &\in S_{p-1}^{-1} \times S_p^1 \\ p &\in S_{p-1}^0 \times S_{p-1}^0 \end{aligned}$$

where the upper index indicates the regularity; for instance -1 indicates that the space is C^{-1}-continuous (or discontinuous). The p in the lower index, here taken to be 2, is the order of the B-splines and must not be mistaken for the pressure p. It will be clear from the context when p means pressure and when it means order.

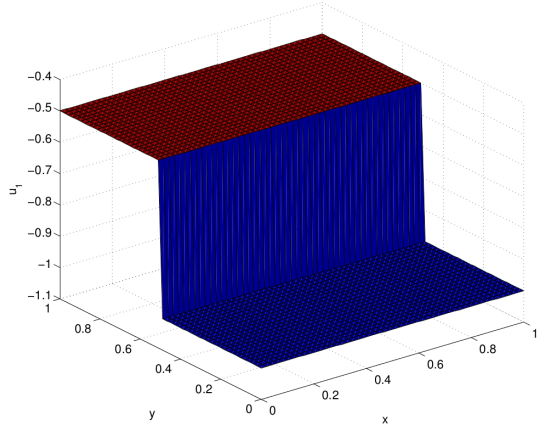

(a) u_1

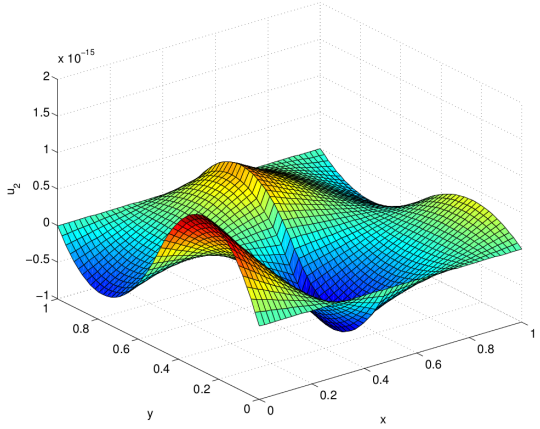

(b) u_2

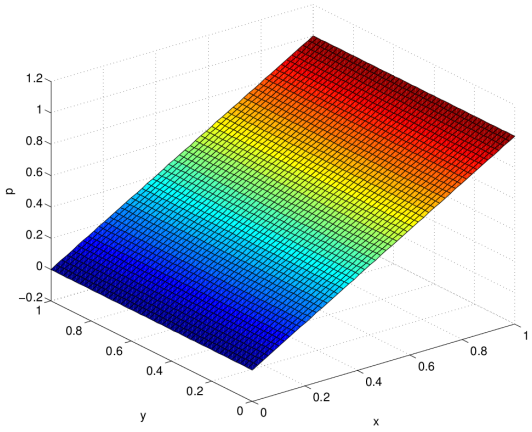

(c) p

Figure 5.2: Plots of the solution to Darcy flow problem with the boundary values as indicated in Figure 5.1. The right hand side function $\mathbf{f}$ is zero. Computed with 33 degrees of freedom, and repeated knots along the boundary between the materials.

A plot of the solution can be found in Figure 5.5. We can observe that u_1 is discontinuous along the line $y = 1/2$, and u_2 is discontinuous along the line $x = 1/2$. Because we now have flow in the y-direction, the pressure is no longer linear, and we can observe these effects in the middle of the domain. These effects would be more visible if the difference in the permeabilities were larger.

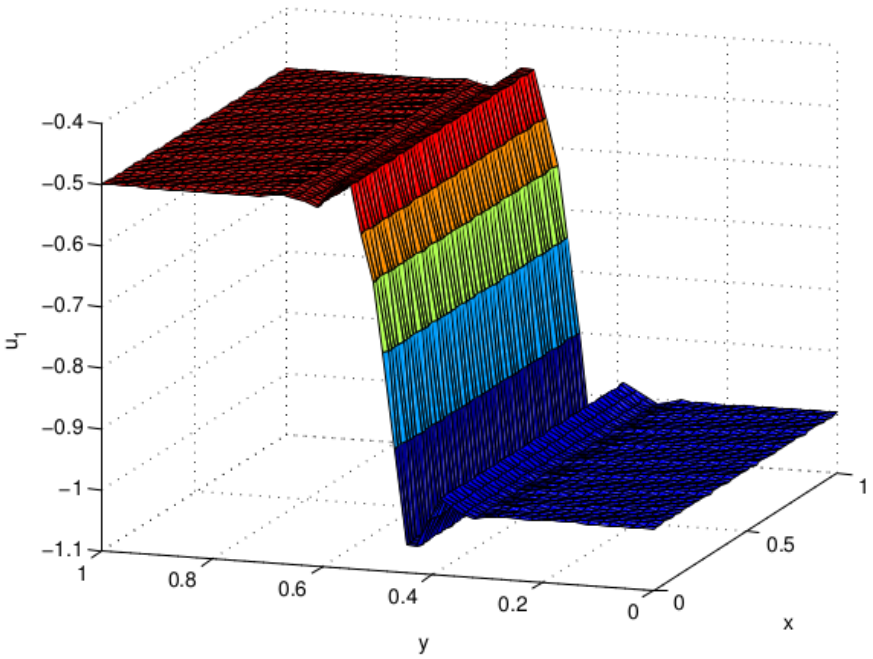

Figure 5.3: Plot of the u_1-solution to Darcy flow problem with the boundary values as indicated in Figure 5.1. The right hand side function $\mathbf{f}$ is zero. Computed with 1121 degrees of freedom, and no repeated knots.

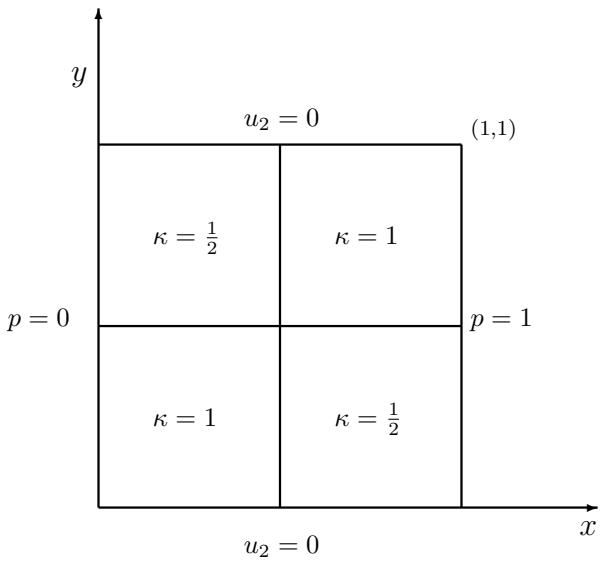

Figure 5.4: Test problem in section 5.2.

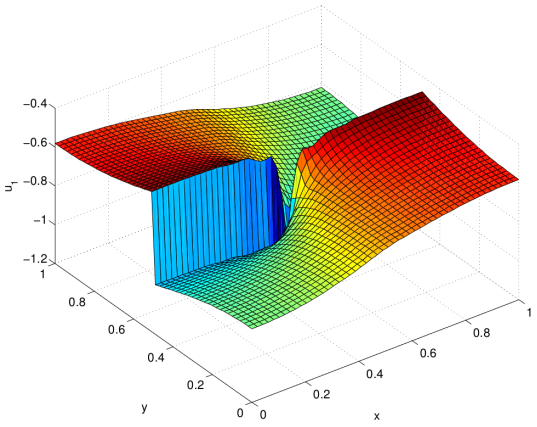

(a) u_1

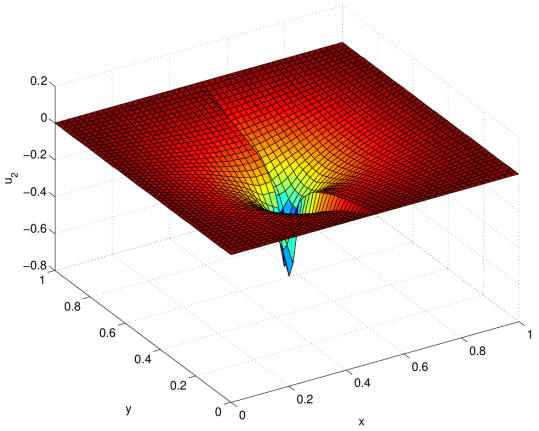

(b) u_2

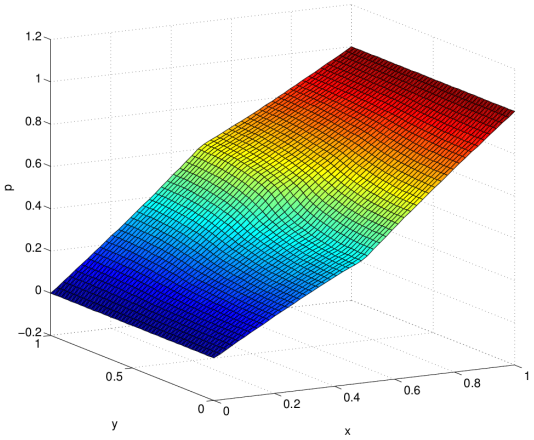

(c) p

Figure 5.5: Plots of the solution to Darcy flow problem with the boundary values as indicated in Figure 5.4. The right hand side function $\mathbf{f}$ is zero. Computed with 1121 degrees of freedom, and repeated knots in both x- and y-direction.

Chapter 6

Concluding remarks

In this thesis we have verified much of the theory presented by Evans [8] regarding compatible B-splines. We have tested the divergence-free property, and have come to the conclusion that the solution is divergence-free in every point when using compatible B-splines as basis functions. This is an important property that the Taylor Hood elements fail to satisfy; at least for a small number of degrees of freedom.

The other main goal of this thesis was to explore the use of repeated knots to obtain discontinuous solutions. This was in order to do simulations on domains with varying permeability with as few elements as possible and still get good results. A few examples have shown us that this is a most promising method for such problems.

All in all this can be made use of in reservoar simulation where flow in porous media is the key problem. In geological models used for these purposes one often let the permeability be constant in each element and therefore there can be a significant change in permeability between elements which again will cause very varying flow velocities. With regular methods such changes will create oscillations in the solution, but with a discontinuous basis this is avoided.

Bibliography

[1] J. Robert Buchanan. Gaussian quadrature, 2006.

[2] A. Buffa, C. de Falco, and G. Sangalli. Isogeometric analysis: Stable elements for 2d stokes equation. *Internasional Journal for Numerical Methods in Fluids*, 2011.

[3] Annalisa Buffa. Compatible discretizations in two dimensions.

[4] J. Austin Cottrell, Thomas J. R. Hughes, and Yuri Bazilevs. *Isogeometric Analysis*. John Wiley & Sons, Ltd, 2009.

[5] Ricardo G. Duran. Mixed finite element methods. http://mate.dm.uba.ar/ rduran/.

[6] V. J. Ervin and E. W. Jenkins. The lbb-condition for the taylor-hood $p_2 - p_1$ and scott-vogelius $p_2 - discp_1$ element pairs in 2-d.

[7] John A. Evans. Divergence-free b-spline discretizations for viscous incompressible flows.

[8] John A. Evans. Phd dissertation proposal: Divergence-free b-spline discretizations for the stokes and navier-stokes equations.

[9] John A. Evans and Thomas J. R. Hughes. Isogeometric divergence-conforming b-splines for the darcy-stokes-brinkman equations, 2012.

[10] John A. Evans and Thomas J. R. Hughes. Isogeometric divergence-conforming b-splines for the steady navier-stokes equations, 2012.

[11] Sven Gross and Arnold Reusken. *Numerical Methods for Two-phase Incompressible Flows*. Springer, 2011.

[12] Mika Juntunen and Rolf Stenberg. Nitsche's method for general boundary conditions. *Mathematics of computation*, 78(267):1353–1374, 2009.

[13] David Kincaid and Ward Cheney. *Numerical Analysis: Mathematics of Scientific Computing*. American Mathematical Society, 3rd edition, 2002.

[14] Tom Lyche and Knut Mørken. Spline methods, 2011.

[15] J. Nitsche. Über ein Variationsprinzip zur Lösung von Dirichlet-Problemen bei Verwendung von Teilräumen, die keinen Randbedingungen unterworfen sind. *Abh. Math. Sem. Univ. Hamburg*, 36:9–15, 1971.

[16] Les Piegl and Wayne Tiller. *The NURBS Book*. Springer, 1995.

[17] David F. Rogers. *An Introduction to NURBS*. Morgan Kaufmann Publishers, 2001.

[18] Daniela Schräder and Holger Wendland. An extended error analysis for a meshfree discretization method of darcy's problem.

[19] Daniela Schräder and Holger Wendland. A high-order, analytically divergence-free discretization method for darcy's problem. *Mathematics of computation*, 2010.

[20] Pavel Solin. *Partial differential equations and the finite element method*. John Wiley and Sons, 2006.